Laue Diffraction and X-Ray Crystallography

Parth Bhargava · A0310667E

PC3193 Experimental Physics II

March 19, 2026

1 Abstract

This two-part experiment uses Laue diffraction and powder X-ray crystallography (XRC) to characterise crystalline materials. Laue patterns recorded for a LiF single crystal show a symmetric spot array consistent with a cubic point group, while patterns for polyethylene monofilament show increased molecular orientation after mechanical drawing. Powder XRC scans of two unknown samples yield indexed peak lists and lattice parameters: Unknown 1 matches a diamond-cubic structure with $a = 5.430 \pm 0.002$ Å (silicon), and Unknown 2 matches a body-centred cubic (BCC) structure with $a = 3.140 \pm 0.004$ Å (molybdenum). The structure factor for the 8-atom diamond-cubic basis is derived to explain the additional selection rules that distinguish diamond-cubic from simple FCC diffraction.

2 Introduction

X-ray wavelengths (≈ 0.5–2.5 Å) are comparable to interatomic spacings in solids, so a crystal acts as a three-dimensional diffraction grating for X-rays. When elastically scattered X-rays from many periodically arranged atoms interfere constructively, discrete diffraction features appear whose geometry encodes the crystal structure. Two complementary methods exploit this.

In **Laue diffraction**, a polychromatic (white) X-ray beam illuminates a single crystal. Each set of lattice planes selects from the continuous spectrum the wavelength that satisfies the Bragg condition, producing a pattern of spots whose symmetry and distribution reveal the crystal's point-group symmetry and orientation. In **powder X-ray crystallography**, a monochromatic beam strikes a polycrystalline sample with randomly oriented crystallites. Each family of planes that satisfies the Bragg condition produces a cone of diffracted radiation; scanning the detector angle 2θ converts these cones into discrete peaks whose positions yield interplanar spacings and, through indexing, the lattice parameters and crystal structure.

The report is organised so that each theoretical development leads directly to a specific measurement and analysis step. The Laue section determines crystal symmetry and orientation from spot patterns; the XRC section identifies two unknown polycrystalline samples from their indexed peak lists and lattice parameters.

3 Theory

3.1 X-Ray Production

X-rays are produced by two mechanisms, each yielding a different spectral character suited to a different diffraction method.

Characteristic X-rays arise when energetic electrons eject inner-shell electrons from target atoms. When outer-shell electrons fill the resulting vacancies, they emit X-rays at discrete energies set by the electronic structure of the target. For a copper anode, the dominant emission is Cu $K_{\alpha 1}$ at $\lambda = 1.5406$ Å. This monochromatic radiation is essential for powder diffraction, where each sharp peak must correspond to a single, well-defined wavelength.

Bremsstrahlung is produced when electrons decelerate in the Coulomb field of target nuclei. The resulting radiation has a continuous spectrum from visible light up to a cutoff energy equal to the electron kinetic energy. This white beam is essential for Laue diffraction, where many wavelengths must be available simultaneously so that every set of lattice planes can find a wavelength satisfying the Bragg condition.

3.2 The Bragg Condition

Consider a set of parallel crystal planes separated by spacing d. When an X-ray beam strikes these planes at a glancing angle θ, rays reflected from successive planes travel different path lengths. Constructive interference occurs when this path difference equals an integer number of wavelengths:

$$n\lambda = 2d\sin\theta \tag{1}$$

This relates the experimentally measured angle 2θ (in a θ-2θ scan) to the interplanar spacing d, which encodes the lattice geometry. Bragg's law underpins both Laue and powder diffraction: in the Laue method, λ is the variable (selected from the white beam); in powder diffraction, θ is the variable (scanned by the goniometer).

3.3 Laue Diffraction

In Laue diffraction, the incident beam contains a continuous range of wavelengths. Each lattice plane (hkl) selects the wavelength λ_{hkl} that satisfies Equation 1 at the fixed geometric angle set by the crystal orientation. The resulting spots on the detector correspond to projections of reciprocal-lattice directions, so the symmetry of the spot pattern mirrors the point-group symmetry of the crystal. For a cubic crystal viewed along a low-index zone axis, the pattern shows the characteristic n-fold rotational symmetry of that axis.

For polymeric samples, Laue patterns reveal the degree of molecular orientation. An amorphous or randomly oriented sample produces diffuse scattering, while a highly oriented (drawn) sample produces sharper, anisotropic features reflecting the preferred alignment of polymer chains along the drawing axis.

3.4 Powder Diffraction and Cubic Indexing

In a polycrystalline powder, crystallites are randomly oriented. For each set of planes satisfying the Bragg condition, a cone of diffracted rays is produced. A θ-2θ scan records intensity as a function of 2θ, converting cones into peaks. Each peak position yields d_{hkl} via Equation 1, and the set of d-values can be indexed to determine the crystal structure.

For cubic crystals with lattice parameter a, the interplanar spacing is:

$$d_{hkl} = \frac{a}{\sqrt{h^2 + k^2 + l^2}} \tag{2}$$

Combining with Equation 1 (for $n = 1$):

$$\sin^2\theta = \frac{\lambda^2}{4a^2}(h^2 + k^2 + l^2) \tag{3}$$

Equation 3 shows that for a cubic crystal, $\sin^2\theta$ increases in proportion to $h^2 + k^2 + l^2$. By computing the ratios of $\sin^2\theta$ values for successive peaks, one can identify the allowed sequence of $h^2 + k^2 + l^2$ values and from that determine the crystal type.

3.5 Structure Factor and Selection Rules

Not all planes produce observable diffraction peaks. The structure factor $F(hkl)$ determines the amplitude of scattering from a unit cell:

$$F(hkl) = \sum_{j=1}^{M} f_j \, \mathsf{exp}\big[2\pi i\big(hx_j + ky_j + lz_j\big)\big] \tag{4}$$

where f_j is the atomic scattering factor and (x_j, y_j, z_j) are the fractional coordinates of the j-th atom. When $F(hkl) = 0$, destructive interference within the unit cell extinguishes the reflection. These are the systematic absences, or selection rules.

Simple cubic (SC): one atom at $(0,0,0)$. $F = f$ for all (hkl), so there are no systematic absences.

Body-centred cubic (BCC): two atoms at $(0,0,0)$ and $(1/2,1/2,1/2)$.

$$F = f\left[1 + e^{i\pi(h+k+l)}\right] = \begin{cases} 2f \text{ if } h+k+l \text{ even} \\ 0 \text{ if } h+k+l \text{ odd} \end{cases} \tag{5}$$

Face-centred cubic (FCC): four atoms at $(0,0,0)$, $(1/2,1/2,0)$, $(1/2,0,1/2)$, $(0,1/2,1/2)$.

$$S_{\mathrm{FCC}} = f\left[1 + e^{i\pi(h+k)} + e^{i\pi(h+l)} + e^{i\pi(k+l)}\right] = \begin{cases} 4f \text{ if } h,k,l \text{ all even or all odd} \\ 0 \text{ otherwise} \end{cases} \tag{6}$$

These selection rules generate distinct sequences of allowed $h^2 + k^2 + l^2$ values:

- **SC:** 1, 2, 3, 4, 5, 6, 8, 9, …
- **BCC:** 2, 4, 6, 8, 10, 12, …
- **FCC:** 3, 4, 8, 11, 12, 16, 19, 20, 24, …

The ratios of successive $\sin^2\theta$ values directly distinguish the three cubic types.

3.6 Diamond-Cubic Structure Factor (8-Atom Basis)

The diamond-cubic structure consists of two interpenetrating FCC sublattices offset by $(1/4,1/4,1/4)$. The 8 atoms in the conventional unit cell occupy:

$$\text{Sublattice 1: } (0,0,0),\ (1/2,1/2,0),\ (1/2,0,1/2),\ (0,1/2,1/2)$$

$$\text{Sublattice 2: } (1/4,1/4,1/4),\ (3/4,3/4,1/4),\ (3/4,1/4,3/4),\ (1/4,3/4,3/4)$$

Sublattice 2 is the same FCC arrangement as sublattice 1, shifted by $(1/4,1/4,1/4)$. The total structure factor is therefore:

$$F(hkl) = S_{\mathrm{FCC}} \cdot \left[1 + e^{i\pi(h+k+l)/2}\right] \tag{7}$$

where S_{FCC} is the FCC structure factor from Equation 6. The second factor $P = 1 + e^{i\pi(h+k+l)/2}$ introduces additional extinctions beyond the FCC rule. Evaluating P for different values of $h+k+l \bmod 4$:

$h+k+l \bmod 4$	$e^{i\pi(h+k+l)/2}$	P	$\lvert F\rvert^2$
0	1	2	$64f^2$
1	i	$1+i$	$32f^2$
2	-1	0	0
3	$-i$	$1-i$	$32f^2$

Table 1: Structure factor magnitude for the diamond-cubic 8-atom basis, evaluated for FCC-allowed reflections only. When $h+k+l \equiv 2 \pmod 4$, the reflection is extinguished by destructive interference between the two sublattices.

The physical consequence is that reflections such as (200) ($h+k+l=2$), (222) ($h+k+l=6$), and (442) ($h+k+l=10$) are forbidden in diamond-cubic but allowed in simple FCC. This additional extinction is what distinguishes diamond-cubic from FCC experimentally.

4 Methods

4.1 Safety and X-Ray Unit

All experiments were performed on enclosed X-ray systems with radiation shielding and interlock mechanisms. X-rays were enabled only with the shield locked in place, and exposure times were controlled by a timer. Tube current was monitored and kept within specified limits.

4.2 Laue Diffraction

LiF single crystal. A LiF mini-crystal was mounted with adhesive tape over the 1 mm diameter primary beam collimator, with the crystal axis aligned at approximately 45°. X-ray film was loaded in the cassette at experimental station E.S. 3, and the pattern was exposed for 40 minutes.

Polyethylene monofilament. A polyethylene monofilament was mounted vertically, centred over the 1 mm collimator port. A first exposure (7 minutes at E.S. 3, 30 kV, 75 µA) recorded the pattern for the undrawn (as-received) filament. The central section was then manually stretched until it acquired a clearly drawn, oriented form, and a second exposure was recorded with the drawn section centred over the beam. The geometry was kept fixed between exposures so that differences in the patterns reflect orientation changes rather than alignment drift.

4.3 Powder X-Ray Crystallography

Two unknown polycrystalline samples were scanned on a PANalytical X'Pert3 powder diffractometer in θ-2θ (goniometer) geometry. The instrument uses a Cu anode with $K_{\alpha 1}$ wavelength 1.5406 Å and $K_{\alpha 2}$ wavelength 1.5444 Å ($K_{\alpha 2}/K_{\alpha 1}$ intensity ratio 0.50). Scans covered $2\theta = 20°$–$140°$ with a step size of 0.02° and 0.40 s per step. The complete instrument settings for each sample are recorded in Table 7. Diffraction data were exported as CSV files for peak identification and indexing.

5 Results

5.1 Laue Diffraction Patterns

The three Laue patterns are shown in Figure 1, Figure 2, and Figure 3.

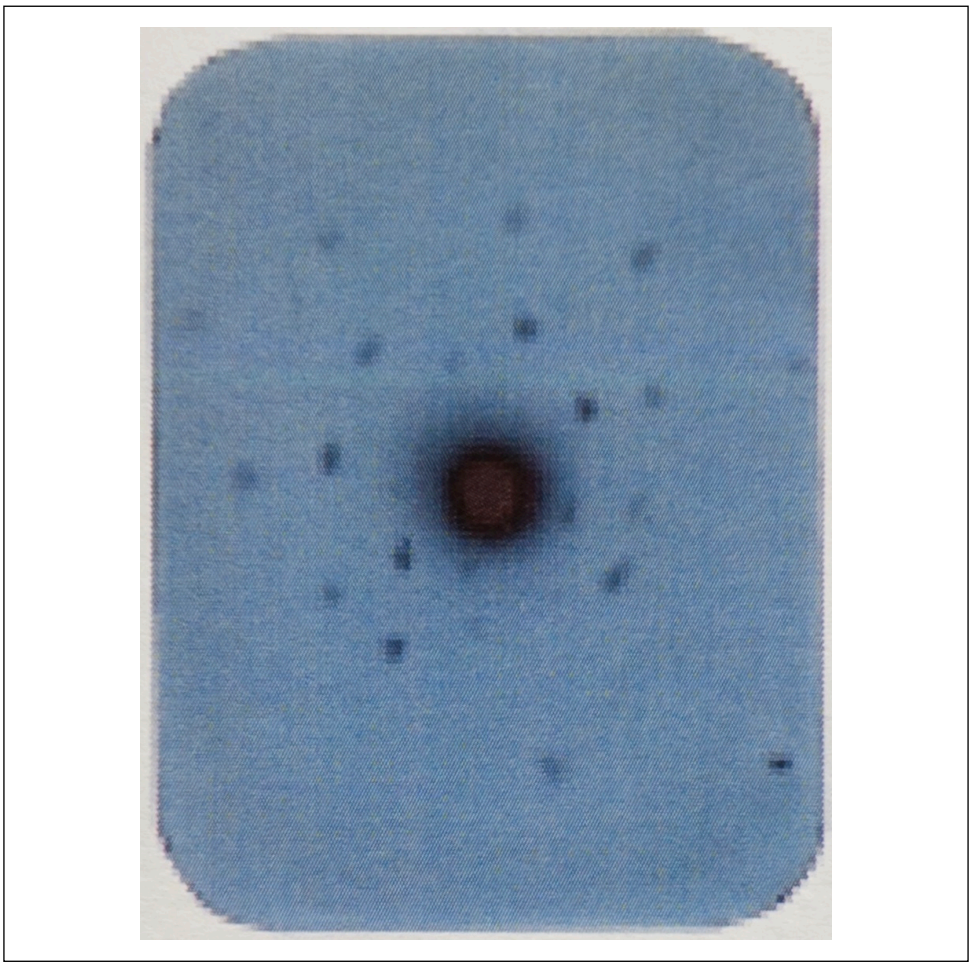

Figure 1: Laue pattern for LiF mini-crystal. Discrete spots arranged with approximate rotational symmetry about the direct beam, consistent with a well-ordered single crystal.

The LiF pattern (Figure 1) shows a set of distinct, well-separated spots distributed symmetrically about the central direct-beam position. The spots appear at discrete angular positions with no diffuse background, confirming that the LiF sample is a well-ordered single crystal with long-range periodicity.

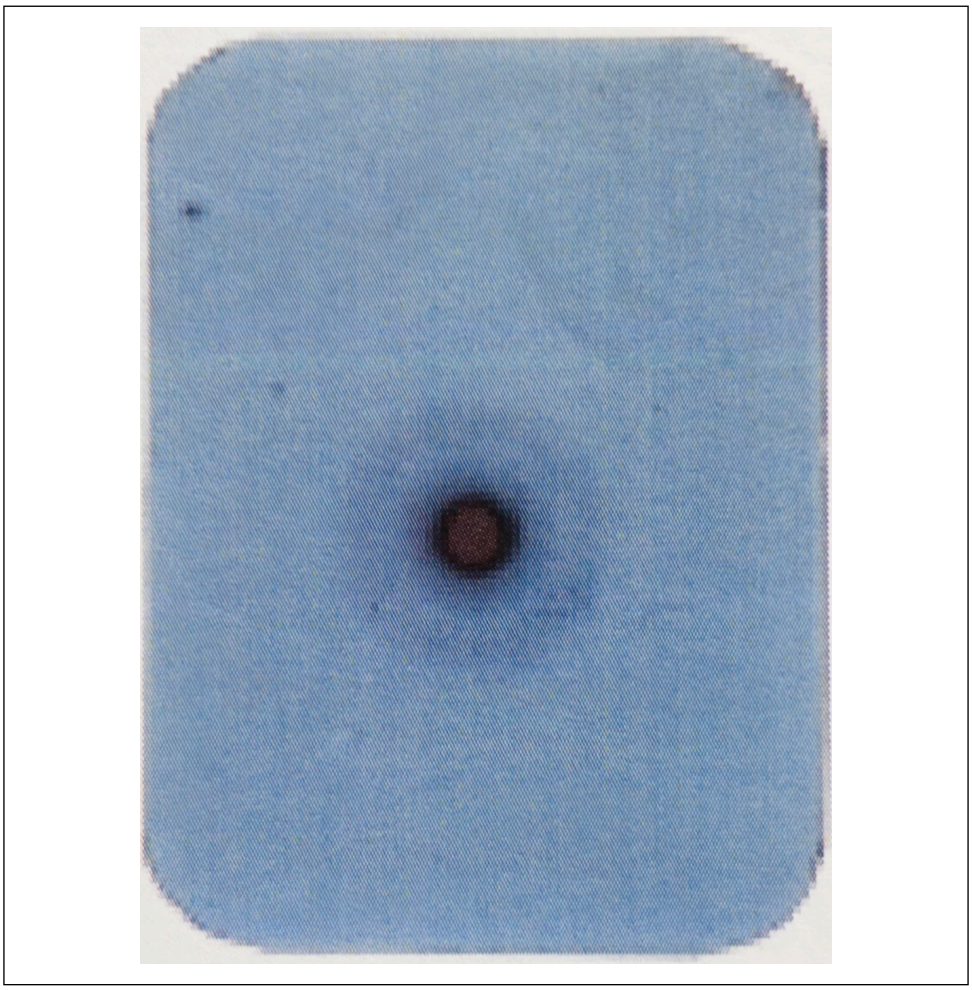

Figure 2: Laue pattern for polyethylene monofilament (undrawn). The diffuse central region and absence of sharp spots indicate low molecular orientation and substantial amorphous character.

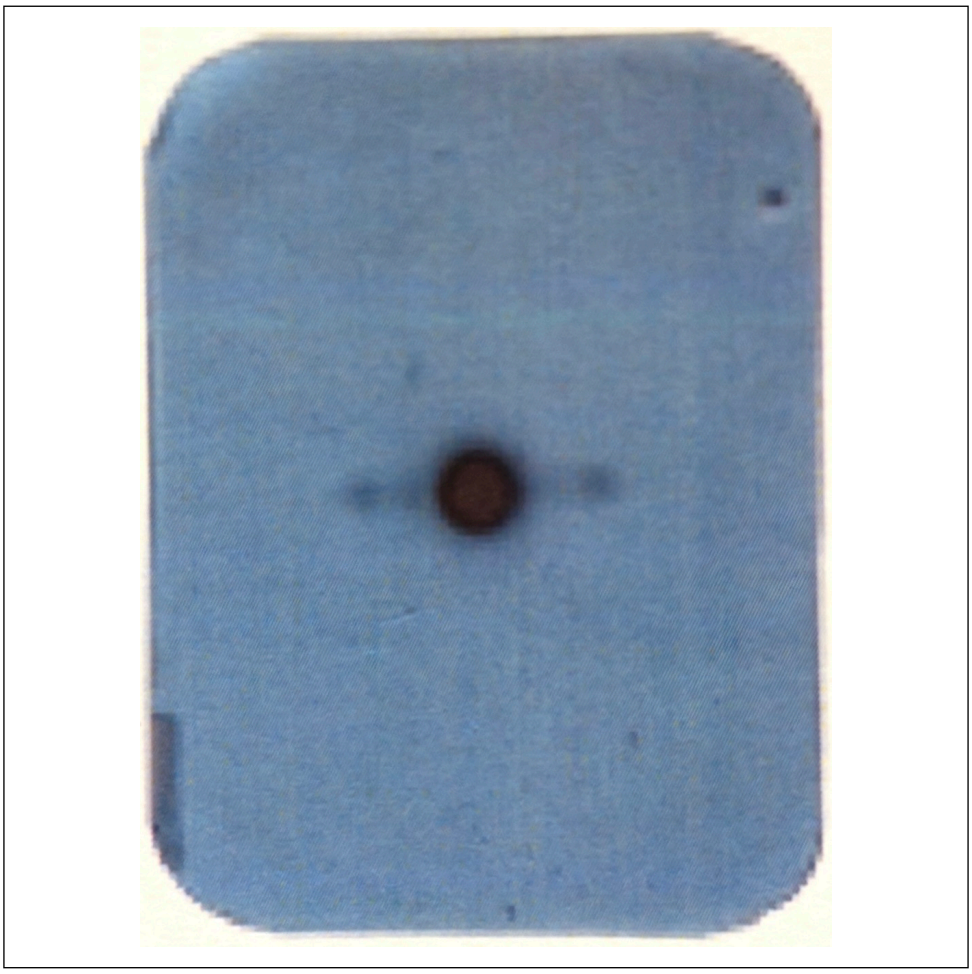

Figure 3: Laue pattern for polyethylene monofilament (drawn). Sharper, axis-aligned features indicate increased molecular orientation along the drawing direction.

The undrawn polyethylene (Figure 2) produces a largely diffuse pattern with no sharp spots, reflecting the lack of long-range crystalline order in the as-received filament. After drawing (Figure 3), the pattern develops sharper features aligned along a preferred axis. The contrast directly shows that mechanical drawing induces molecular alignment: the polymer chains, initially oriented randomly, become preferentially parallel to the draw axis, introducing enough order to produce anisotropic diffraction.

5.2 XRC Scans

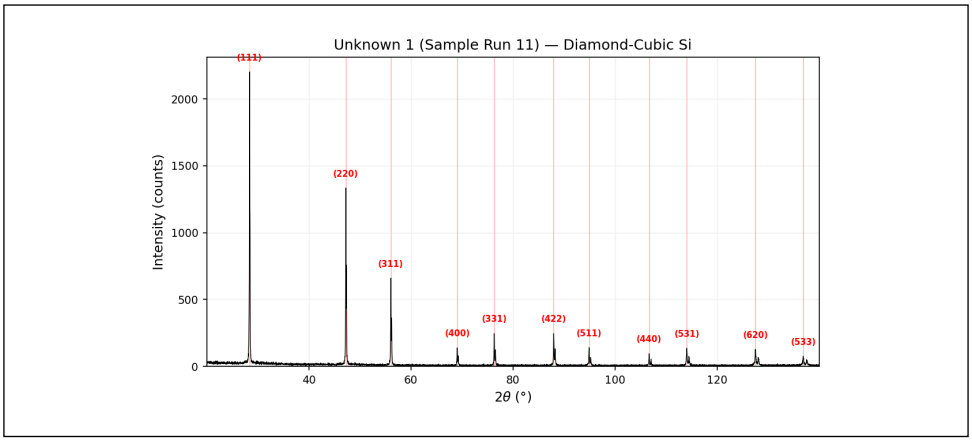

Figure 4: Powder XRC scan for Unknown 1 (Sample Run 11). The dominant peak at $2\theta \approx 28.4°$ is the (111) reflection. All observed peaks are consistent with diamond-cubic selection rules.

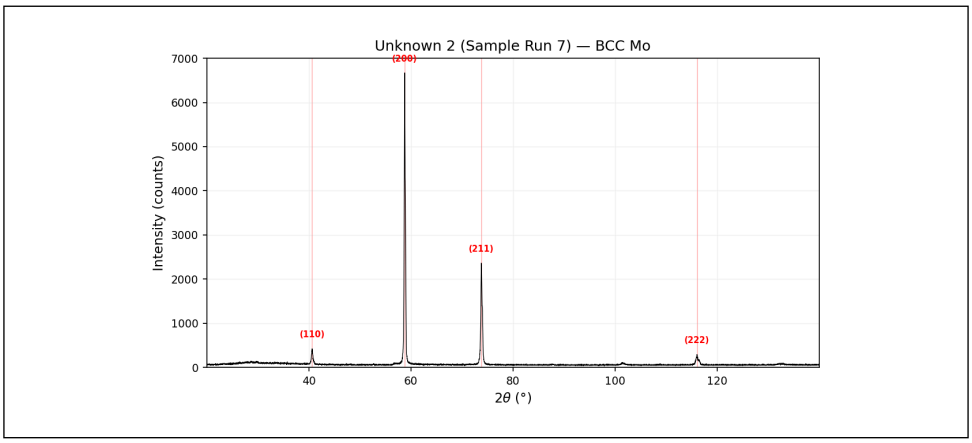

Figure 5: Powder XRC scan for Unknown 2 (Sample Run 7). The dominant peak at $2\theta \approx 58.8°$ is the (200) reflection under BCC indexing. Several weak features in the 26°–34° range sit at or near the noise floor and do not index consistently with the main phase; these are attributed to amorphous background scattering from the sample holder.

The indexed peak lists for both unknowns are presented in Table 2. Peak positions were determined from the scan data after smoothing and thresholding. Interplanar spacings were computed from each peak using Bragg's law ($d = \lambda/(2\sin\theta)$) with $\lambda = 1.5406$ Å.

Sample	**2θ (°)**	**Intensity**	**(hkl)**	**d (Å)**	**a (Å)**
Unknown 1	28.43	2201	(1 1 1)	3.137	5.433
Unknown 1	47.33	525	(2 2 0)	1.919	5.428
Unknown 1	56.15	256	(3 1 1)	1.637	5.427
Unknown 1	69.11	139	(4 0 0)	1.358	5.432
Unknown 1	76.35	246	(3 3 1)	1.246	5.430
Unknown 1	88.01	246	(4 2 2)	1.109	5.431
Unknown 1	94.93	140	(5 1 1)	1.045	5.430
Unknown 1	106.69	95	(4 4 0)	0.960	5.430
Unknown 1	114.07	129	(5 3 1)	0.918	5.431
Unknown 1	127.53	122	(6 2 0)	0.859	5.431
Unknown 1	136.89	71	(5 3 3)	0.828	5.430
Unknown 2	40.67	353	(1 1 0)	2.217	3.135
Unknown 2	58.81	6318	(2 0 0)	1.569	3.138
Unknown 2	73.83	2238	(2 1 1)	1.283	3.142
Unknown 2	116.07	292	(2 2 2)	0.908	3.145

Table 2: Indexed peak list for the two unknown samples. Each peak's d-spacing is computed from Bragg's law with $\lambda = 1.5406$ Å, and the lattice parameter a is derived from Equation 2. Unknown 1 is indexed as diamond-cubic; Unknown 2 as BCC.

6 Analysis

6.1 Laue Symmetry and Orientation

The LiF Laue pattern shows approximately 20–25 discrete spots distributed about the central direct-beam position, with no diffuse background. The spots are sharp and well-separated, confirming single-crystal quality and stable orientation throughout the 40-minute exposure. The pattern exhibits approximate mirror symmetry about at least one axis, consistent with a high-symmetry cubic crystal.

LiF crystallises in the rock-salt (NaCl-type) structure with space group $Fm\bar{3}m$, which belongs to the cubic point group $m\bar{3}m$ and possesses two-, three-, and four-fold rotation axes. Since the crystal was mounted with its axis at approximately 45° to the beam, the incident direction does not coincide with a principal zone axis ($\langle 100\rangle$, $\langle 110\rangle$, or $\langle 111\rangle$), and the observed pattern is therefore a general projection of the reciprocal lattice rather than one showing the full rotational symmetry of a specific zone. The overall arrangement of spots is nevertheless consistent with a cubic crystal of high symmetry.

For polyethylene, the transition from diffuse scattering (undrawn) to anisotropic features (drawn) shows the mechanical induction of crystallographic texture. In the undrawn state, crystalline lamellae are randomly oriented, producing no preferred diffraction directions. Drawing forces the polymer chains into approximate alignment along the draw axis, creating a fibre texture where the c-axis of the orthorhombic polyethylene unit cell aligns preferentially along the fibre direction. In effect, the drawn filament behaves as a partially oriented polycrystal.

6.2 XRC Indexing: $\sin^2\theta$ Ratio Method

The first step in powder pattern analysis is to determine the crystal type from the sequence of observed reflections. Computing $\sin^2\theta$ for each peak and forming ratios relative to the first peak reveals the allowed values of $h^2 + k^2 + l^2$, which immediately identifies the structure type.

6.2.1 Unknown 1

The $\sin^2\theta$ values for the first six peaks of Unknown 1 are:

2θ (°)	$\sin^2\theta$	Ratio	$h^2+k^2+l^2$	(hkl)
28.43	0.0606	1.00	3	(1 1 1)
47.33	0.1614	2.66	8	(2 2 0)
56.15	0.2222	3.67	11	(3 1 1)
69.11	0.3226	5.32	16	(4 0 0)
76.35	0.3833	6.32	19	(3 3 1)
88.01	0.4844	7.99	24	(4 2 2)

Table 3: Ratio analysis for Unknown 1. The sequence 3, 8, 11, 16, 19, 24 matches the FCC-allowed values with the additional absence of $h^2 + k^2 + l^2 = 4$ (i.e. the (200) reflection), which is the signature of diamond-cubic structure.

The ratio sequence $1 : 2.66 : 3.67 : 5.32 : 6.32 : 7.99$ corresponds to $h^2 + k^2 + l^2 = 3$, 8, 11, 16, 19, 24. This matches the FCC selection rule (all even or all odd indices), but with the notable absence of (200) ($h^2 + k^2 + l^2 = 4$) and (222) ($h^2 + k^2 + l^2 = 12$). These additional absences are precisely the extinctions predicted by the diamond-cubic structure factor (Table 1): reflections with $h + k + l \equiv 2 \pmod 4$ vanish because of destructive interference between the two FCC sublattices.

The lattice parameters computed from each peak cluster tightly around $a = 5.430 \pm 0.002$ Å, in excellent agreement with the literature value for silicon ($a = 5.431$ Å). Unknown 1 is therefore identified as **silicon** with the diamond-cubic structure.

6.2.2 Unknown 2

The $\sin^2\theta$ analysis for the four strong peaks of Unknown 2 gives:

2θ (°)	$\sin^2\theta$	Ratio	$h^2+k^2+l^2$	(hkl)
40.67	0.1208	1.00	2	(1 1 0)
58.81	0.2409	1.99	4	(2 0 0)
73.83	0.3606	2.98	6	(2 1 1)
116.07	0.7190	5.95	12	(2 2 2)

Table 4: Ratio analysis for Unknown 2. The sequence 2, 4, 6, 12 is a subset of the BCC-allowed values ($h+k+l$ even), confirming a body-centred cubic structure.

The ratios $1 : 2.00 : 2.98 : 5.95$ correspond to $h^2+k^2+l^2 = 2, 4, 6, 12$. This is the signature of a BCC lattice, where the selection rule $h+k+l =$ even eliminates reflections such as (100), (111), (210), and (311). The missing values 8 and 10 (which would correspond to (220) and (310)) are expected at $2\theta \approx 87°$ and $\approx 101°$. For BCC, all allowed reflections share the same structure-factor magnitude $|F|^2 = 4f^2$, so the absence of these peaks is not a selection-rule effect. Rather, their expected intensities are suppressed by the combination of lower multiplicity at high $h^2+k^2+l^2$, the Lorentz-polarization factor $\frac{1}{\sin^2\theta\cos\theta}$ which reduces high-angle intensities, and the Debye–Waller factor e^{-2M} which further attenuates peaks at large scattering angles. Together these effects place (220) and (310) below the detection threshold of this scan.

Several weak peaks appear in the 26°–34° range of the Unknown 2 scan (intensities around 110–140, compared to the strongest peak at 6318). These do not index consistently with the BCC phase ($\sin^2\theta$ ratios do not match the BCC sequence) and are likely from minor surface contamination or background scattering from the sample mount.

The lattice parameters from the four indexed peaks give $a = 3.140 \pm 0.004$ Å (σ of individual values), which identifies the material as **molybdenum** ($a_{\text{lit}} = 3.147$ Å, 0.2% discrepancy). However, the individual a values show a systematic trend: 3.135, 3.138, 3.142, 3.145 Å for the (110), (200), (211), (222) reflections respectively — monotonically increasing with 2θ. This is the classic signature of a small positive zero-angle offset $\Delta(2\theta)$ in the goniometer. A positive offset shifts all measured 2θ values upward, which depresses d (and hence a) more strongly at low angles where $\frac{d(\sin\theta)}{d}\theta$ is smaller. Extrapolating a to $\theta \to 90°$ (where the zero-offset effect vanishes) would yield a value closer to the literature 3.147 Å. The Si data show a much tighter spread (5.427–5.433 Å) because Si has 11 peaks spanning a wider 2θ range, and the random peak-position uncertainty ($\pm 0.02°$ step size) dominates over the systematic offset.

Sample	Mean a (Å)	Structure	Identification
Unknown 1	5.430 ± 0.002	Diamond cubic	Silicon
Unknown 2	3.140 ± 0.004	BCC	Molybdenum

Table 5: Summary of lattice parameters and structural identification.

6.3 Verification via Diamond-Cubic Selection Rules

The identification of Unknown 1 as diamond-cubic silicon is further supported by checking the 8-atom basis selection rules from Equation 7 and Table 1 against the full peak list.

The observed reflections for Unknown 1 have $h+k+l$ values of 3, 4, 5, 4, 7, 8, 7, 8, 9, 8, 11, all satisfying $h+k+l \not\equiv 2 \pmod 4$. Crucially, the (200) reflection ($h+k+l = 2$) and (222) reflection ($h+k+l = 6$) are absent despite being allowed by the simpler FCC rule. This is exactly the extinction pattern one would get from the second FCC sublattice shifted by $(1/4, 1/4, 1/4)$, confirming a diamond-cubic basis rather than simple FCC.

For a simple FCC metal (aluminium, copper, gold), the (200) reflection would be one of the strongest peaks. Its complete absence in the Unknown 1 pattern, together with the lattice parameter matching silicon, leaves no ambiguity in the identification.

6.4 $K_{\alpha1}/K_{\alpha2}$ Doublet Splitting

At high 2θ, the Cu $K_{\alpha1}$ ($\lambda = 1.5406$ Å) and $K_{\alpha2}$ ($\lambda = 1.5444$ Å) lines are resolved as separate peaks. Differentiating Bragg's law, the angular separation for a doublet is $\Delta(2\theta) = \frac{2\Delta\lambda \cos\theta}{\lambda \sin\theta}$, which diverges as $\theta \to 90°$. The Unknown 1 (Si) data provide five clearly resolved doublet pairs:

(hkl)	$2\theta_{K\alpha1}$ (°)	$2\theta_{K\alpha2}$ (°)	$\Delta(2\theta)_{\text{obs}}$ (°)	$\Delta(2\theta)_{\text{calc}}$ (°)
(3 3 1)	76.35	76.57	0.22	0.22
(4 2 2)	88.01	88.27	0.26	0.27
(5 1 1)	94.93	95.25	0.32	0.32
(5 3 1)	114.07	114.51	0.44	0.47
(6 2 0)	127.53	128.11	0.58	0.64

Table 6: Observed and calculated $K_{\alpha1}/K_{\alpha2}$ doublet separations for Si. Calculated values use $\Delta\lambda = 0.0038$ Å and the Bragg-law derivative. Agreement confirms the peak positions are instrumentally resolved and not artefacts.

The monotonic increase of $\Delta(2\theta)$ with angle is consistent with theory. The small discrepancies at the highest angles ($\approx 0.06°$ at $2\theta = 128°$) reflect the difficulty of resolving the weaker $K_{\alpha2}$ component when it overlaps with the tail of the $K_{\alpha1}$ peak. The $K_{\alpha2}$ intensities are approximately half those of $K_{\alpha1}$, as expected from the literature ratio of 0.50.

7 Discussion

7.1 Laue vs. Powder Diffraction

The Laue and XRC results illustrate two fundamentally different uses of X-ray diffraction. The Laue method, with its white beam and fixed geometry, gives qualitative information about crystal symmetry and orientation. The powder method, with its monochromatic beam and scanned angle, gives quantitative information about lattice parameters and structure type.

For the Laue results, the contrast between the LiF single-crystal pattern and the polyethylene patterns illustrates the difference between long-range crystalline order (producing discrete spots) and the partial order induced by mechanical processing (producing anisotropic diffuse scattering). The drawn polyethylene pattern does not show the sharp spots of a single crystal because the polymer remains polycrystalline; the anisotropy comes from preferred orientation of crystalline lamellae, which in metallurgical terms is called fibre texture.

7.2 Indexing and Identification

The $\sin^2\theta$ ratio method gives an unambiguous distinction between crystal types without requiring any prior knowledge of the material. The ratio sequence 3, 8, 11, 16, … immediately points to FCC-type reflections, while the additional absence of $h^2 + k^2 + l^2 = 4$ narrows the identification to diamond-cubic. For Unknown 2, the ratio sequence 2, 4, 6, 12 directly identifies BCC, ruling out both FCC and simple cubic. The lattice parameters then match the structures to specific elements.

7.3 Peak Intensities and Structure Factor

For diamond-cubic Si, the strongest reflection is (111) ($I \approx 2200$ counts), followed by (220) (≈ 1350), (311) (≈ 700), and rapidly diminishing higher-order peaks. This ordering is broadly consistent with theoretical expectations: the structure factor for Si alternates between $|F|^2 = 64f^2$ for reflections where $h + k + l = 4n$ (e.g., (220), (400)) and lower values for others, but the **observed** intensity

is modulated by the multiplicity p and the Lorentz-polarization factor $L_p = \frac{1+\cos^2 2\theta}{\sin^2\theta\cos\theta}$. The (111) reflection is strongest despite $|F_{111}|^2 < |F_{220}|^2$ because the L_p factor at low 2θ (28.4°) is $\approx 7\times$ larger than at 47.3°.

For BCC Mo, the (200) reflection dominates (≈ 6600 counts), which at first sight is surprising because all BCC reflections share $|F|^2 = 4f^2$. The explanation is again the L_p factor: (200) at 58.8° sits near the minimum of the L_p curve but has multiplicity $p = 6$, while (211) at 73.8° has $p = 24$ but is penalised by larger Debye–Waller attenuation. The (110) reflection (≈ 400 counts) is anomalously weak relative to its L_p advantage at 40.7°, which may reflect texture or preferred orientation in the powder sample.

7.4 Systematic Zero-Offset in Lattice Parameters

The dominant source of uncertainty in the XRC analysis is peak-position determination, which depends on step size (0.02°), counting statistics, and any systematic zero-angle offset. As noted in Section 6.2.2, the Mo lattice parameter increases monotonically from 3.135 Å at (110) to 3.145 Å at (222), a clear signature of a positive $\Delta(2\theta)$ zero-offset. The effect is described by:

$$a_{\text{obs}} = a_{\text{true}}\left(1 - \frac{\Delta(2\theta)}{2\tan\theta}\right) \tag{8}$$

so the correction is largest at small θ (i.e. low-angle peaks yield the most depressed a). A Nelson-Riley extrapolation — plotting a against the function $\frac{1}{2}\left(\cos^2\frac{\theta}{\sin}\theta + \cos^2\frac{\theta}{\theta}\right)$ and extrapolating to zero — would give the best estimate of a_{true}. The four-point Mo data are too sparse for a reliable extrapolation, but the trend is qualitatively consistent with $\Delta(2\theta) \approx +0.04°$, which would bring the mean a from 3.140 to ≈ 3.146 Å, very close to the literature value of 3.147 Å.

The Si lattice parameters cluster tightly (5.427–5.433 Å, $\sigma = 0.003$ Å) because the 11 indexed peaks span a wide 2θ range (28°–137°), so the positive and negative deviations from a_{true} partially cancel in the mean.

7.5 Background Features in Unknown 2

The Unknown 2 spectrum shows a broad, weak hump between $2\theta \approx 26°$ and 34°. This feature does not correspond to any BCC Mo reflection (the lowest-angle allowed peak is (110) at 40.7°). It is most likely an amorphous scattering halo from the glass sample holder or from a thin oxide layer on the powder surface. Amorphous SiO_2 glass produces a broad peak centred near $2\theta \approx 22°$–28° for Cu K_α radiation, consistent with the observed position. This background was excluded from the indexing and does not affect the lattice parameter determination.

8 Conclusion

The Laue patterns confirm single-crystal symmetry for LiF and show that mechanical drawing induces molecular orientation in polyethylene. The powder XRC scans yield internally consistent indexed peak lists for both unknowns: Unknown 1 is diamond-cubic silicon ($a = 5.430$ Å) and Unknown 2 is BCC molybdenum ($a = 3.140$ Å). The 8-atom diamond-cubic structure factor derivation accounts for the additional extinctions (absence of (200) and (222) reflections) that distinguish silicon from a simple FCC metal. The BCC identification of Unknown 2 is established by the $\sin^2\theta$ ratio sequence $1 : 2 : 3 : 6$ and the lattice parameter match to molybdenum.

9 References

1. Laue Diffraction, PC3193 manual (provided).
2. X-Ray Crystallography, PC3193 manual (provided).
3. C. Kittel, *Introduction to Solid State Physics*, 8th ed. (Wiley, 2005), Chapter on Diffraction.
4. H.P. Myers, *Introductory Solid State Physics* (Taylor & Francis, 1997).

10 Appendix

10.1 Instrument Settings

Parameter	**Unknown 1 (Run 11)**	**Unknown 2 (Run 7)**
Diffractometer	PANalytical X'Pert3	PANalytical X'Pert3
Goniometer	PW3050/60 (θ/θ)	PW3050/60 (θ/θ)
Geometry	Flat sample stage (PW3071/xx)	Flat sample stage (PW3071/xx)
Anode material	Cu	Cu
$K_{\alpha 1}$ wavelength	1.5406 Å	1.5406 Å
$K_{\alpha 2}$ wavelength	1.5444 Å	1.5444 Å
Generator voltage	40 kV	45 kV
Tube current	30 mA	40 mA
Scan range (2θ)	20.0°–140.0°	20.0°–140.0°
Step size	0.020°	0.020°
Scan type	Continuous	Continuous
Time per step	0.40 s	0.40 s
Divergence slit	Fixed, 1.52 mm	Fixed, 1.52 mm
Receiving slit	0.10 mm	0.10 mm
Monochromator	No	No
No. of points	6000	6000
Scan date	15 Feb 2024	8 Oct 2025

Table 7: XRC instrument settings for the two unknown samples, extracted from the measurement metadata.

10.2 Laue Exposure Log

Sample	**Station**	**Exposure time**	**Tube settings**
LiF mini-crystal	E.S. 3	40 min	Standard (1 mm collimator, 45° alignment)
Polyethylene (undrawn)	E.S. 3	7 min	30 kV, 75 µA
Polyethylene (drawn)	E.S. 3	7 min	30 kV, 75 µA

Table 8: Exposure parameters for Laue diffraction patterns.

11 Declaration on the Use of Generative AI

I declare that I **HAVE** used generative AI tools to produce this assignment.

I acknowledge that generative AI was used in the following manner:

AI Tool Used	**My Prompt and AI Output**	**How the Output Was Used**
Claude Code	**Prompt:** "Help me process the powder XRD data files, identify peaks, calculate $\sin^2\theta$ ratios, and determine lattice parameters for the unknown samples." **Output:** Python script for peak extraction and lattice parameter calculation	Used for data processing automation. All diffraction measurements were recorded by me, and the identification of crystal structures through systematic absence analysis and lattice parameter comparison is my own work.
Claude Code	**Prompt:** "Help with Typst formatting for figures, tables, equations, and appendix layout. Check that cross-references and file paths compile correctly." **Output:** Typst formatting guidance and layout suggestions	Used only for formatting. All experiment content, analysis, and scientific interpretations were written and verified by me.

Table 9: AI Tool Usage Declaration